Eur. Phys. J. D **9**, 137–140 (1999)

THE EUROPEAN PHYSICAL JOURNAL D

EDP Sciences

Lattice contraction in nanosized silicon particles produced by laser pyrolysis of silane

H. Hofmeister[1,a], F. Huisken[2], and B. Kohn[2]

[1] Max-Planck-Institut für Mikrostrukturphysik, Weinberg 2, D-06120 Halle,Germany
[2] Max-Planck-Institut für Strömungsforschung, Bunsenstrasse 10, D-37073 Göttingen, Germany

Received: 31 August 1998 / Received in final form: 3 December 1998

Abstract. We used laser-induced decomposition of silane for the fabrication of nanosized Si particles and studied in detail their structural characteristics by conventional and high resolution electron microscopy. The silane gas flow reactor incorporated in a molecular beam apparatus was operated without size selection to achieve a broad size distribution. Deposition at low energy on carbon substrates yielded single crystalline, spherical Si particles almost completely free of planar lattice defects. The particles, covered by thin amorphous oxide shells, are not agglomerated into larger aggregates. The lattice of diamond cubic type exhibits deviations from the bulk spacing which vary from distinct contraction to dilatation as with decreasing particle size the oxide shell thickness is reduced. This effect is discussed in terms of the strong Si/oxide interfacial interaction and compressive stresses arising upon oxidation. A negative interface stress, as determined from the size dependence of the lattice spacing, limits the curvature of the interface, i.e., at small sizes Si oxidation must be considered as a self-limiting process.

PACS. 61.16.-d Electron, ion, and scanning probe microscopy – 61.46.+w Clusters, nanoparticles, and nanocrystalline materials – 81.05.-t Specific materials: fabrication, treatment, testing and analysis

1 Introduction

Silicon based particulates having structural characteristics on the nanometer scale exhibit promising optoelectronic properties, e.g., photoluminescence in the visible range, that result from size-induced quantum confinement effects in close relationship to surface passivation by Si−O bonds [1]. Besides erosive surface techniques widely used to process bulk silicon [2, 3], there is growing interest in gas phase synthesis of nanosized Si particles which, by embedding them in a passivating matrix, may be stabilised against influences of the ambient. Various methods of synthesis are reported ranging from co-sputtering of Si and silica, ion implantation of Si into silica, laser ablation and gas phase evaporation of silicon to plasma-assisted decomposition of silane [4–10]. New hints to the self-limiting nature of oxide formation at nanosized Si particles were obtained from Si particles produced by inert gas arc evaporation [11].

The capabilities of laser vaporisation sources have been employed for generating cluster beams of materials of low vapour pressure since more than ten years [12]. A recently developed novel cluster source [13] yielding well defined, narrowly dispersed particles [14] has proven to be particularly well suited for the aim of particle fabrication. The apparatus combines laser-induced decomposition of silane gas in a flow reactor with size selection in the neutral cluster beam and mass detection in a time-of-flight mass spectrometer (TOFMS). In addition to previously presented in-situ gas phase characterisation as well as photoluminescence and Raman investigations of such Si particles [15, 16], high resolution electron microscopy (HREM) is now employed for structural characterisation of the corresponding particles down to the atomic scale.

2 Experimental

The Si particles were generated by laser-induced decomposition of silane in a gas flow reactor that has been described in detail elsewhere [13–16]. Silane gas flushed with helium is admitted to the centre of the reactor where the gas flow is crossed by a pulsed CO_2 laser beam. The flow reactor is situated in the source chamber of a molecular beam machine equipped with a TOFMS. The reaction products are extracted through a conical nozzle into vacuum and then pass through a skimmer into the deposition chamber which precedes the TOFMS chamber. Carbon coated microgrids placed on a sampling probe 30 cm downstream from the nozzle exit served to collect the particles from the cluster beam with or without size selection by a rotating chopper wheel. In a typical experiment the reactor was operated under the following conditions: 40 sccm flow rate of silane, 1100 sccm flow rate of helium, 350 mbar

[a] Corresponding author. e-mail: `hof@mpi-halle.mpg.de`

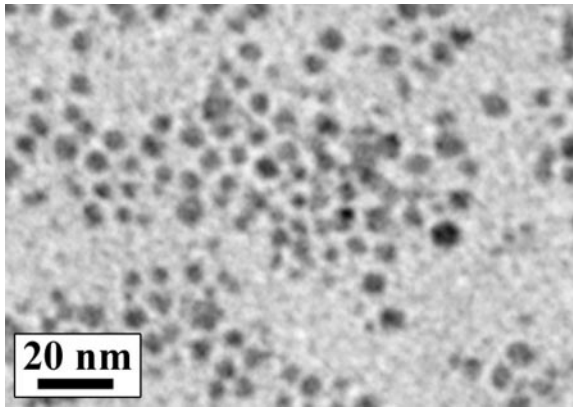

Fig. 1. Si particles randomly assembled on the supporting carbon film.

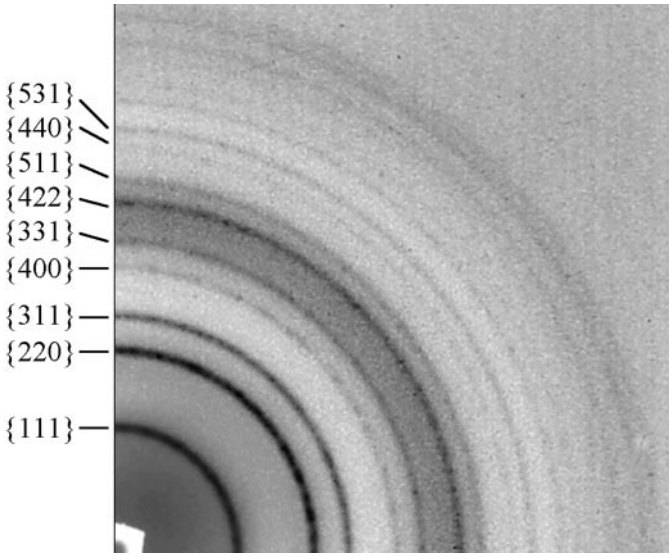

Fig. 2. SAED pattern of a typical layer of Si particles with the Miller indices of diffraction rings indicated.

total pressure, and 50 mJ CO_2 laser pulse energy. No intentional oxidation treatment was applied to the Si particles, but trace amounts of oxygen possibly present in the gas flow reactor and in the deposition chamber cannot be excluded. For structural characterisation by transmission electron microscopy (TEM) a conventional JEM 100C operated at 100 kV and a high resolution electron microscope JEM 4000EX operated at 400 kV were used. The HREM images were recorded at optimum imaging conditions (near Scherzer focus). Particle size, oxide shell thickness and the spacing of lattice plane fringes were determined from digitised HREM micrographs by digital image processing and evaluation using the Digital Micrograph (GATAN) and NIH Image [17] software.

3 Results

Under the conditions mentioned above laser induced decomposition of silane yields spherical particles with diameters between 2 and approximately 25 nm. Remarkably, they do not agglomerate into larger aggregates as it is known from other routes of synthesis [8–11]. Instead, the deposits consist of separated particles, covering at random the substrates used for collection and being stacked onto each other upon prolonged deposition. Figure 1 shows a selection of a typical layer. The corresponding selected area electron diffraction (SAED) pattern shown in Fig. 2 includes well established diffraction rings down to a lattice plane spacing of less than 0.1 nm according to the diamond cubic lattice of silicon together with diffuse intensity from amorphous material. The latter is identified to result from the carbon support as well as silicon oxide.

As may be recognised from Fig. 3, which shows two Si particles without support (sticking to the edge of a hole in the carbon film), the particles consist of a crystalline core completely covered by an amorphous shell probably being silicon oxide. For particles deposited on amorphous carbon films, the thickness of the oxide shell cannot be determined. Thus, the sizes determined from HREM micrographs refer to the dimensions of the crystalline core

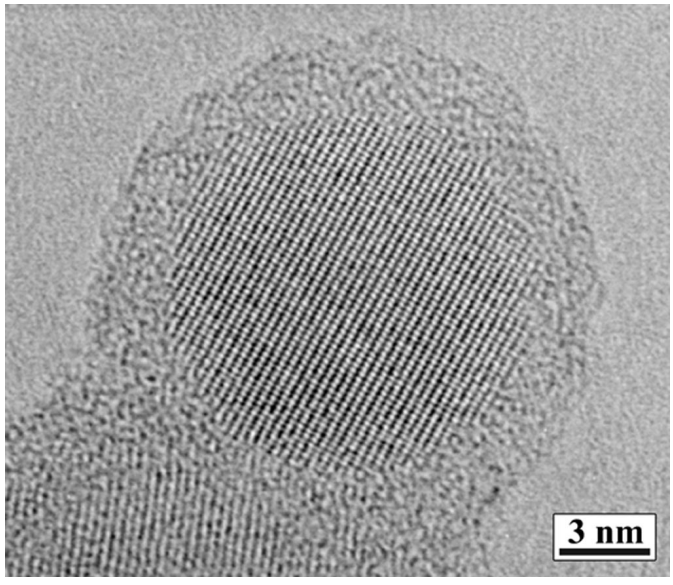

Fig. 3. HREM image of single crystalline Si particles sticking to the edge of a hole in the carbon film. Their coating by amorphous oxide shells may clearly be recognised.

only. The corresponding size distribution is given in Fig. 4. From images such as shown in Fig. 3 (only about 0.1% of all particles imaged), the thickness of the oxide layer can be determined. The result of this evaluation is shown in Fig. 5. It is seen that the thickness of these oxide shells linearly decrease from about 2.9 to 0.8 nm when the particle size is reduced from 33 to 6 nm.

The particles are single crystalline and almost completely free of planar lattice defects. According to lattice structure analysis by means of the reciprocal space representation (diffractogram) of digitised HREM images, the lattice of diamond cubic type exhibits distinctly reduced spacing as compared to the bulk value for particles larger

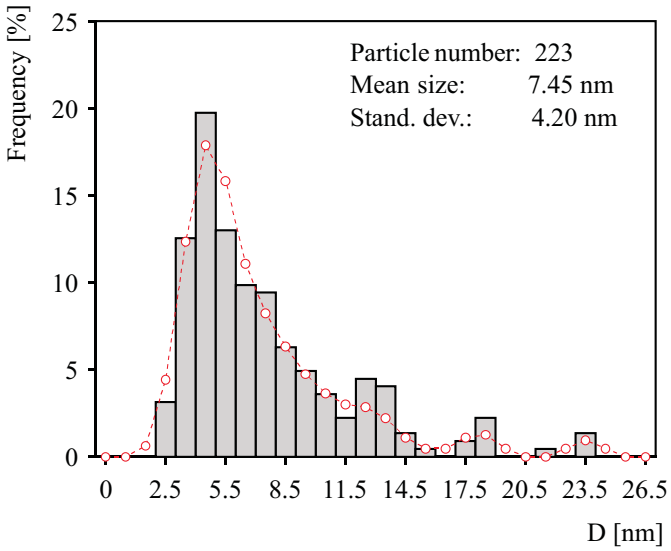

Fig. 4. Particle size distribution as determined from crystalline core dimensions.

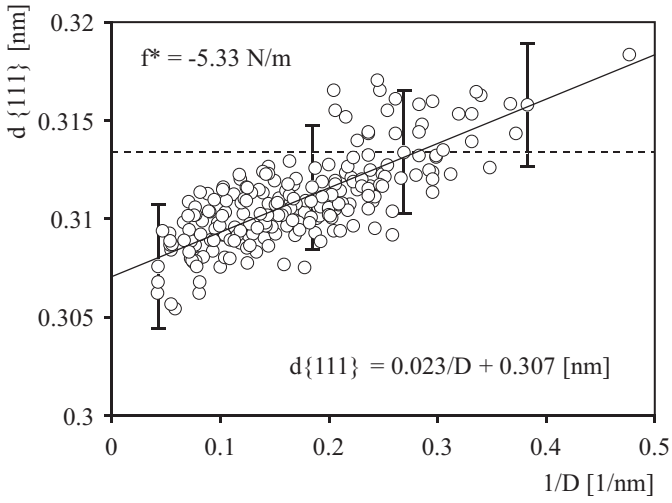

Fig. 6. Spacing of {111} lattice plane fringes as a function of the reciprocal particle size. The broken line corresponds to the d{111} bulk value.

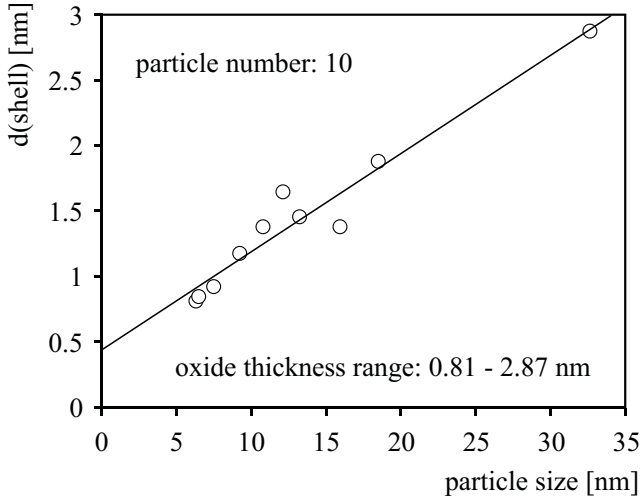

Fig. 5. Oxide shell thickness as function of the actual particle size.

than about 3 nm (crystalline core diameter). This lattice compression diminishes for decreasing particle size and changes to lattice dilation for particles smaller than about 3 nm, as is demonstrated by the plot of the spacing of the {111} lattice plane fringes versus the reciprocal particle diameter shown in Fig. 6.

4 Discussion

The present electron microscopy investigation of the Si particles revealed structural characteristics related to the peculiarities of nanostructured silicon and the conditions of synthesis applied. Different from other observations at Si-based particulates [8–11] no particle agglomeration was found which may be due to the rapid transfer of particles from the reaction zone into high vacuum, directly after formation. This 'dilution' procedure obviously prevents the formation of larger aggregates in the cluster beam.

The formation of amorphous surface oxide on Si and Ge particles of a few nm to a few 100 nm in size has been reported in a number of publications [11, 18–20]. Size effects were determined with respect to the oxide composition [18, 19] as well as to the oxidation rate [20], i.e., with decreasing particle size an increasing oxygen deficiency and a decreasing oxidation rate, respectively, were observed. The latter effect was also demonstrated for Si nanowires of conical shape [21]. Oxidation may set in even in vacuum at a relatively low oxygen partial pressure of about 4×10^{-8} mbar [22, 23]. A core/shell structure was also deduced for deposited Si clusters upon oxygen adsorption [24]. Therefore we consider the oxidation of our Si particles likewise to result from oxygen exposure starting already in vacuum and being continued by their exposure to the ambient. Taking into account the storage under ambient conditions and the dependence of the oxide shell thickness on the particle size (see Fig. 5), we expect it to correspond to the respective saturation configuration.

The state of stress of the Si particles monitored by their respective lattice spacing may be interpreted in terms of the formation of a new phase, i.e., the surface oxide or the formation of a Si/oxide interface. With the formation of oxide at the particle surface compressive stress to accommodate the volume expansion arises that may attain values of several GPa [21], hence enabling lattice contraction of the observed extent. The stress at the Si/oxide interface ought to diminish with decreasing oxide thickness. While this applies to planar Si structures, it may fail with nonplanar structures of nanometer size.

To describe the effect of the Si/oxide interface on nonplanar Si nanostructures we first consider particles free of surface oxide. Owing to the surface curvature, small particles are in a state of compression. For the cubic lattice type the resulting reduction of lattice spacing $\triangle a$ is given

by the Laplace-type equation

$$\triangle a = -2fa\kappa/3r \quad (1)$$

where f is the surface stress, a the bulk lattice parameter, κ the compressibility, and r the particle radius. Small particles coated by a shell of foreign material may be treated as particles embedded in a matrix where the surface stress is replaced by the interface stress f^*. Accordingly, size dependent changes of the lattice spacing are determined by value and sign of the interface stress. From (1) and from the size dependence of the lattice spacing (see linear regression in Fig. 6), an interface stress of -5.33 N/m is derived, indicating a strong interaction. This value is within the range of experimental and theoretical data reported for the surface stress due to the adsorption of oxygen on Si(111) single crystal surfaces [22]. The particularly large scatter of data may be due to variations in the oxide stoichiometry and to non-homogeneous oxide coverage of the particles.

The interface stress representing the elastic response of the interface to elastic deformation is determined by the strength of interaction (adhesion work) of the phases adjacent to the interface according to

$$W_{\mathrm{adh}} = f(\mathrm{shell}) + f(\mathrm{core}) - f^* \quad (2)$$

If the strength of interaction in a system of phases exceeds the sum of the respective surface stress values, the interface stress may attain negative values. A negative interface stress limits the curvature the interface can withstand for energetical reasons. Since the process of silicon oxide formation requires the interface to move towards the silicon phase it will stop at a certain value of interface curvature. This is the reason that the oxide thickness decreases with decreasing particle size. Consequently, for small particle sizes the oxidation of silicon must be considered as a self-limiting process.

5 Summary

CO_2-laser driven pyrolysis of silane has been used to produce a molecular beam of nanosized Si particles which were deposited on holey carbon films. Structural characterisation by HREM revealed these particles to be of high crystallinity and perfection. Amorphous oxide shells, completely covering the particles, cause lattice contractions which diminish with decreasing oxide thickness and decreasing particle size, changing to lattice dilatation at small particle sizes. These findings provide useful information for understanding and predicting the oxidation behaviour of non-planar Si nanostructures. In particular, the optoelectronic properties of oxide passivated Si nanoparticles should be concerned, since the electron density of states in nanosized Si particles may severely be influenced by lattice parameter changes of the observed type.

F.H. and B.K. gratefully acknowledge support from the Deutsche Forschungsgemeinschaft.

References

1. H. Tamura, M. Rückschloss, T. Virschem, S. Veprek: Thin Solid Films **255**, 92 (1995)
2. U. Gösele, V. Lehmann: Mater. Chem. Phys. **40**, 253 (1995)
3. M.H. Ludwig, A. Augustin, R.E. Hummel, T. Gross: J. Appl. Phys. **80**, 5318 (1996)
4. M. Zacharias, D. Dimova-Malinovska, M. Stutzmann: Philos. Mag. B **73**, 799 (1996)
5. T. Shimizu-Iwayama, S. Nakao, K. Saitoh: Nucl. Instrum. Methods Phys. Res., Sect. B **120**, 97 (1996)
6. I.A. Movtchan, R.W. Dreyfus, W. Marine, M. Sentis, M. Autric, G. Le Lay, N. Merk: Thin Solid Films **255**, 286 (1995)
7. L.N. Dihn: Phys. Rev. B **54**, 5029 (1996)
8. H. Hofmeister, J. Dutta, H. Hofmann: Phys. Rev. **54**, 2856 (1996)
9. H. Hofmeister, P. Ködderitzsch, U. Gösele: Ber. Bunsenges. Phys. Chem. **101**, 1647 (1997)
10. H. Hofmeister, P. Ködderitzsch, J. Dutta: J. Non-Cryst. Solids **232**–**234**, 182 (1998)
11. H. Hofmeister, P. Ködderitzsch: Nanostructured Materials, in press, vol. 12 (1999)
12. J.R. Heath, Y. Liu, S.C. O'Brien, Q.-L. Zhang, R.F. Curl, F.K. Tittel, R.E. Smalley: J. Chem. Phys. **83**, 5520 (1985)
13. M. Ehbrecht, H. Ferkel, V.V. Smirnov, O.M. Stelmakh, W. Zhang, F. Huisken: Rev. Sci. Instrum. **66**, 3833 (1995)
14. M. Ehbrecht, H. Ferkel, F. Huisken: Z. Phys. D **40**, 88 (1997)
15. M. Ehbrecht, B. Kohn, F. Huisken, M.A. Laguna, V. Paillard: Phys. Rev. B **56**, 6958 (1997)
16. M. Ehbrecht, F. Huisken: Phys. Rev. B **59**, 2975 (1999)
17. W. Rasband: 'NIH Image', public domain software, US National Institute of Health (FTP: zippy.nimh.nih.gov)
18. S. Hayashi, S. Tanimoto, K. Yamamoto: J. Appl. Phys. **68**, 5300 (1990)
19. S. Hayashi, S. Tanimoto, M. Fujii, K. Yamamoto: Superlattices Microstruct. **8**, 13 (1990)
20. R. Okada, S. Iijima: Appl. Phys. Lett. **58**, 1662 (1991)
21. H.I. Liu, D.K. Biegelsen, N.M. Johnson, F.A. Ponce, R.F.W. Pease: J. Vac. Sci. Technol. B **11**, 2532 (1993)
22. D. Sander, H. Ibach: Phys. Rev. B **43**, 4263 (1991)
23. S. Hayashi, S. Kawata, H.M. Kim, K. Yamamoto: Jpn. J. Appl. Phys. **32**, 4870 (1993)
24. J.E. Bower, M.F. Jarrold: J. Chem. Phys. **97**, 8312 (1992)